Structures and Properties of 1,8,15,22-Tetrasubstituted Phthalocyaninato-Lead Complexes: The Substitutional Effect Study Based on Density Functional Theory Calculations

Yuexing Zhang,[†] Xianxi Zhang,[†,‡] Zhongqiang Liu,[†,§] Yongzhong Bian,[†] and Jianzhuang Jiang*[,†]

Department of Chemistry, Shandong University, Jinan 250100, P.R. China, School of Chemistry and Chemical Engineering, Liaocheng University, Liaocheng 252059, P.R. China, and Department of Material, Shandong Institute of Light Industry, Jinan 250100, P.R. China

Received: March 5, 2005; In Final Form: April 30, 2005

Density functional theory (DFT) and time-dependent DFT calculations were carried out to comparatively describe the molecular structures, molecular orbital energy gaps, atomic charges, infrared (IR) and Raman spectra, and UV−vis spectra of PbPc (**1**), PbPc(α-OC_2H_5)$_4$ (**2**), and PbPc(α-OC_5H_{11})$_4$ (**3**) {Pc^{2-} = dianion of phthalocyanine; [Pc(α-OC_2H_5)$_4$]$^{2-}$ = dianion of 1,8,15,22-tetra-ethoxyphthalocyanine; [Pc(α-OC_5H_{11})$_4$]$^{2-}$ = dianion of 1,8,15,22-tetrakis(3-pentyloxy)phthalocyanine}. The calculated structural data of compounds **1** and **3** and the simulated IR and UV−vis spectra of **3** are compared with X-ray crystallography molecular structures and the experimental absorption spectra respectively to verify the performance of the B3LYP method and the LANL2DZ basis set. Substitution of bulky alkoxy groups at the nonperipheral positions of the phthalocyanine ring adds obvious effect to the molecular structure of phthalocyaninato lead compounds by deflecting the isoindole units in the direction that the isoindole units extends and distorting them in the C_4 axis direction due to the steric hindrance. Both the calculated IR and UV−vis absorption spectra of **3** correspond well with the experimental results.

Introduction

Phthalocyanines are of great interest in science and industry due to their peculiar and unconventional chemical and physical properties.[1] They have been important dyes and pigments since their early synthesis at the beginning of the last century.[1−3] In recent years, the phthalocyanine derivatives have also been used as charge carriers in photocopiers and laser printers and materials for optical storage.[4−7] Many potential applications are expected for these molecular materials which have high thermal and chemical stability, such as oxidation catalysts,[8] solar cell functional materials,[9,10] gas sensors,[11,12] nonlinear optical limiting devices,[13−15] photodynamic therapy agents,[16,17] antimycotic materials,[18] and corrosion inhibitors.[19]

Phthalocyanines can form complexes with almost all of the metals in the periodic table. The structures and properties of these metal complexes can thus be altered by changing the central metal. The other way to tune the structures and properties of phthalocyanine compounds is to introduce different species of substituents onto the peripheral and nonperipheral positions of the phthalocyanine ring. In particular, the structures, electronic and spectroscopic properties, and orbital gaps can be significantly altered by incorporating different substituents at the nonperipheral positions of phthalocyanines. This has been well demonstrated by our recent work on the 1,8,15,22-tetrakis-(alkoxy)phthalocyanine-containing bis- and tris-(phthalocyaninato) metal complexes, namely M(Pc)[Pc(α-OC_5H_{11})$_4$] (M = Y, Sm−Lu) and (Pc)M(Pc)M[Pc(α-OC_5H_{11})$_4$] (M = Sm, Gd, Lu).[20−22] It is worth noting that due to the C_4 symmetry of the Pc(α-OC_5H_{11})$_4$ ring and the sandwich-like structure, the molecules of these sandwich-type double- and triple-decker complexes are intrinsically chiral in nature, also possessing a C_4 symmetry as revealed by the X-ray molecular structural analysis results.[20−22]

Among the various metal elements in the periodic table, lead has been relatively little studied for complexation with phthalocyanines in either experiments or theoretic calculations despite the potential uses of these complexes as nonlinear optical materials. Studies have been mainly focused on the unsubstituted analogues,[23−27] whereas only a few substituted phthalocyaninato lead(II) complexes have been reported so far.[28,29] Herein we describe the molecular structures, molecular orbital energy gaps, atomic charges, IR and Raman spectra, and the UV−vis electronic absorption spectra of two lead complexes of phthalocyanines tetrasubstituted at the nonperipheral positions in comparison with those of unsubstituted phthalocyanine analogue with the help of DFT calculations.

With the development of the computer industry and calculation method, the calculation and simulation of large molecules and even supramolecules with more than 100 atoms are possible. Semiempirical molecular orbital calculations using PM3 Hamiltonian have been employed to assist the qualitative assignments of the vibrational spectrum of zinc phthalocyanine (ZnPc) in 1999.[30] Gong had studied the structure and properties of the *tert*-butyl substituted phthalocyanines in 2002.[31] Just in the last year Liao and co-workers reported the effects of peripheral substituents and axial ligands on the electronic structure and properties of iron phthalocyanine.[32] Density functional theory (DFT) methods, which include electron correlation effects, have proved suitable for the energy-minimized structure calculations of H_2Pc and its metal derivatives.[31−33]

* Corresponding author. Tel.: +86-531-856-4088. Fax: + 86-531-856-5211. E-mail: jzjiang@sdu.edu.cn.
[†] Shandong University.
[‡] Liaocheng University.
[§] Shandong Institute of Light Industry.

10.1021/jp0511449 CCC: $30.25
Published on Web 06/28/2005

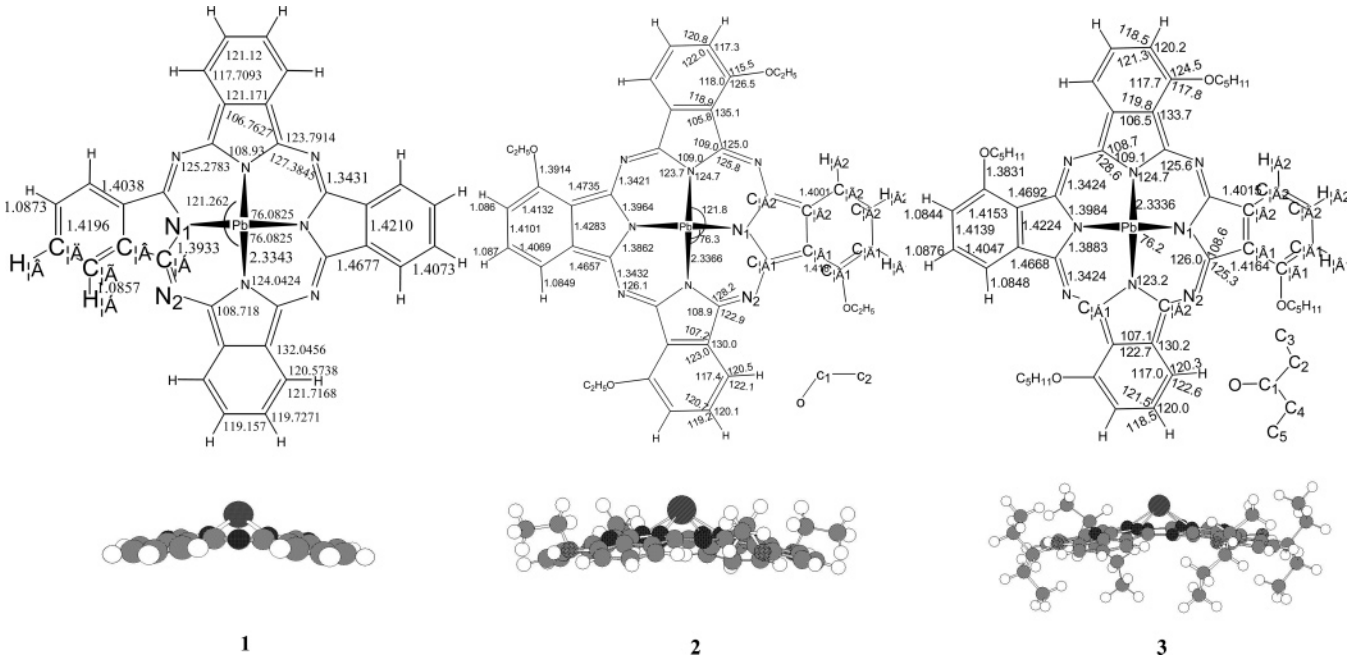

Figure 1. Calculated structures and main structure parameters of PbPc (**1**), PbPc(α-OC_2H_5)$_4$ (**2**), and PbPc(α-OC_5H_{11})$_4$ (**3**).

In the present paper, we studied the molecular structures, molecular orbital energy gaps, atomic charges, IR and Raman spectra, and UV−vis spectra of three lead phthalocyaninates, PbPc (**1**), PbPc(α-OC_2H_5)$_4$ (**2**), and PbPc(α-OC_5H_{11})$_4$ (**3**). The DFT method B3LYP was used to calculate the structures and vibrational properties of **1**−**3** with LANL2DZ basis set and the time-dependent DFT (TDDFT) method with the same basis set the electronic absorption spectra. The calculated structures of **1** and **3** and the simulated IR and UV−vis spectra of **3** are compared with the reported experimental results. To the best of our knowledge, this appears to be the first report dealing with the detailed structures and spectroscopic properties of the lead complexes with the nonperipherally tetrasubstituted phthalocyanine obtained at density functional theory level.

Computational Details

The primal input structure of **1** was obtained from the result of our previous calculations, in which the Pb^{2+} ion was put into the central cavity of the phthalocyanine dianion and the molecular structure was optimized using a small basis set and a cheap method. For compounds **2** and **3**, four ethyloxy and 3-pentyloxy groups were introduced to the 1,8,15,22-nonoperipheral positions of compound **1** as the primal inputs, respectively. The hybrid density functional B3LYP (Becke-Lee-Young-Parr composite of exchange-correlation functional) method was used for both geometry optimizations and property calculations. In all cases, the LANL2DZ basis set was used. It is worth mentioning that the molecules of all of the three complexes **1**−**3** cannot be studied using a small level basis set [even including the widely used "bigger" 6-31G and 6-31G(d) basis set] because of the complexity of the electronic shell of the lead atom involved. Therefore, the LANL2DZ basis set (D95 on first row elements, Los Alamos ECP plus DZ on Na−Bi) is selected for the calculations in the present work. The Berny algorithm using redundant internal coordinates[34] was employed in energy minimization and the default cutoffs were used throughout. C_4 symmetry for compounds **2** and **3**, and C_{4v} for **1**, in the input structures were detected and then enforced by the program. Using the energy-minimized structures generated in the previous step, normal coordinate analyses were carried out. Charge distribution is carried out using a full natural bond orbital analysis (NBO) population method based on the minimized structure. The primarily calculated vibrational frequencies were scaled by the factor 0.9614.[35] UV−vis spectroscopic calculations were made by TDDFT method. All calculations were carried out using the Gaussian 03 program[36] in the IBM NAS 300 system in Shandong Province High Performance Computing Centre.

Results and Discussion

Molecular Structure. The energy-minimized structures optimized at the B3LYP/LANL2DZ level are C_{4v} symmetry for **1** and C_4 symmetry for **2** and **3**, indicating the intrinsic chirality of molecules of the latter two complexes. This is in line with the experimental result.[28] As revealed by the X-ray single-crystal molecular structure of **3**, the lead ion is too big to completely enter the central cavity of the phthalocyanine ring but sits atop of the ligand, and the resulting molecule having a C_4 symmetry thus possesses an intrinsic chirality. All of the compounds **1**−**3** have a nonplanar "shuttle-cock" structure with the lead ion being the cork hemisphere and the phthalocyanine ligand being the attaching feathers and the substituents being the additional feathers at the tail end of the attaching feathers, Figure 1.[37] It is noteworthy that the fact that no imaginary vibration is predicted in the following frequency calculations of the IR and Raman vibrational spectroscopy indicates that the energy-minimized structures for all of the three complexes are true energy minimums. The structure parameters of our minimum-energy geometry for **1**−**3** not only agree with previous calculations[33] but also are in good accordance with the experimental values.[28,38,39]

Table 1 compares our calculated structure parameters of PbPc (**1**) with the X-ray crystallography data of its monoclinic and triclinic form[38,39] and the result calculated by Papageorgiou.[40] The differences between the experimental and calculated data in the structure parameters of **1** are shown in Figure 2. As can be seen, the calculated Pb−N_1 bond length is 0.1243 Å longer than that found in the monoclinic crystal and 0.0257 Å shorter than that in the triclinic crystal, revealing the good agreement in the structural data obtained by the DFT method with

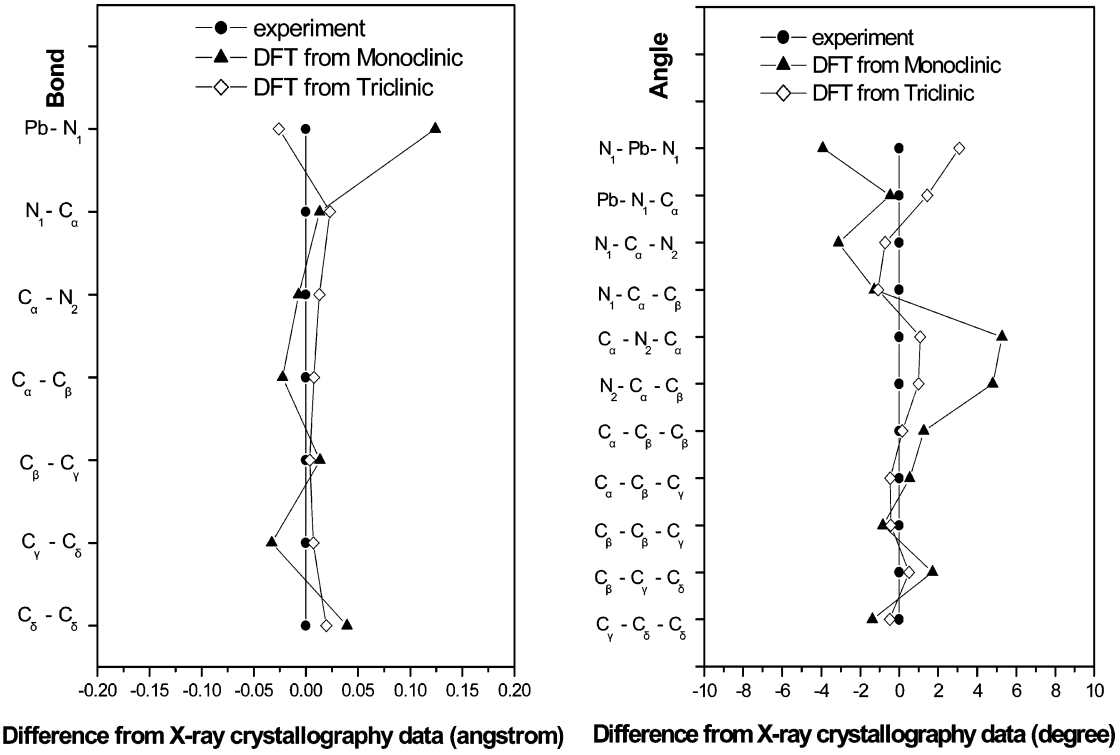

Figure 2. Comparison of main calculated bond lengths and bond angles with the X-ray crystallography data for PbPc (**1**).

TABLE 1: Experimental and Calculated Main Structure Parameter of PbPc (1)

parameter[a]	monoclinic[b]	triclinic[b]	Papageorgiou's work[c]	calculated[d]
Pb−N_1	2.21	2.36	2.43	2.3343
N_1−C_α	1.38	1.37	1.37	1.3933
C_α−N_2	1.35	1.33	1.33	1.3431
C_α−C_β	1.49	1.46	1.46	1.4677
C_β−C_γ	1.39	1.4	1.39	1.4038
C_γ−C_δ	1.44	1.4	1.4	1.4073
C_δ−C_δ	1.38	1.4	1.41	1.4196
N_1−Pb−N_1	80	73	72.3	76.0825
Pb−N_1−C_α	124.5	122.6	123	124.0424
N_1−C_α−N_2	130.5	128.1	128	127.3845
N_1−C_α−C_β	110	109.8	108.5	108.718
C_α−N_2−C_α	120	124.2	124.7	125.2783
N_2−C_α−C_β	119	122.8	123.2	123.7914
C_α−C_β−C_β	105.5	106.6	106.6	106.7627
C_α−C_β−C_γ	131.5	132.5	132.4	132.0456
C_β−C_β−C_γ	122.0	121.6	121	121.171
C_β−C_γ−C_δ	116	117.2	117.8	117.7093
C_γ−C_δ−C_δ	122.5	121.6	121.1	121.12

[a] N_1: nitrogen atom joined to the central metal; N_2: nitrogen atom not joined to the central metal; $\alpha\ \beta\ \gamma\ \delta$ mean carbon atoms in isoindole units beginning from N_1. (see Figure 1). [b] Data taken from refer 38 and 39. [c] Data taken from refer 40. [d] Calculated data with the B3LYP/LANL2DZ method(see also Figure 1).

TABLE 2: Experimental and Calculated Main Structure Parameter of PbPc(α-OC_5H_{11})$_4$ (3)

parameter[a]	expt.[b]	calc.[c]	parameter[a]	expt.[b]	calc.[c]
Pb−N_1	2.3758	2.3336	$C_{\gamma1}$−O	1.3548	1.3831
N_1−$C_{\alpha1}$	1.3698	1.3984	O−C_1	1.4470	1.4848
N_1−$C_{\alpha2}$	1.3495	1.3883	C_1−C_2	1.5200	1.5398
$C_{\alpha1}$−$C_{\beta1}$	1.4683	1.4692	C_2−C_3	1.4568	1.5414
$C_{\alpha2}$−$C_{\beta2}$	1.4528	1.4668	C_1−C_4	1.4980	1.5395
$C_{\beta1}$−$C_{\gamma1}$	1.3983	1.4164	C_4−C_5	1.4810	1.5405
$C_{\beta2}$−$C_{\gamma2}$	1.3853	1.4015	N_1−Pb−N_1	72.5	76.2
$C_{\beta1}$−$C_{\beta2}$	1.4005	1.4224	$C_{\alpha1}$−N_1−$C_{\alpha2}$	109.1	109.1
$C_{\gamma1}$−$C_{\delta1}$	1.3863	1.4153	N_1−$C_{\alpha1}$−$C_{\beta1}$	108.7	108.6
$C_{\gamma2}$−$C_{\delta2}$	1.3738	1.4047	N_1−$C_{\alpha2}$−$C_{\beta2}$	109.8	108.7
$C_{\delta1}$−$C_{\delta2}$	1.3820	1.4139	$C_{\alpha1}$−N_2−$C_{\alpha2}$	122.9	125.6
$C_{\alpha1}$−N_2	1.3300	1.34241	$C_{\gamma1}$−O−C_1	119.6	123.1
$C_{\alpha2}$−N_2	1.3373	1.34239	C_2−C_1−C_4	112.0	112.5

[a] N_1: nitrogen atom joined to the central metal; N_2: nitrogen atom not joined to the central metal; $\alpha\ \beta\ \gamma\ \delta$ mean carbon atoms in isoindole units beginning from N_1; the subscript 1 on carbon atom refer to carbon atoms at the same side of oxygen atom, the subscript 2 on carbon atom refer to carbon atoms at the contrary side of oxygen atom, the same to hydrogen atoms; C_1: carbon atom in substituents joined to oxygen atom, C_2 and C_4 both joined to C_1 atom and C_2 C_3 at the same side of lead atom, C_4 and C_5 at the other side for *c* molecular.(see Figure 1); Å for bond length and degree for bond angle. [b] Data taken from refer 28. [c] Calculated data with B3LYP/LANL2DZ method (see also Figure 1 **3**).

experimental results. However, according to Papageorgiou,[40] their calculated Pb−N bond length is overestimated compared with that in both the monoclinic and triclinic crystals. Moreover, the data shown in Figure 2 also clearly indicate that our calculated structure results agree much better with those in the triclinic crystal than in the monoclinic one. For instance, the biggest difference in the bond angle of our calculated data from that in the monoclinic crystal is 5.2783° for C_α−N_2−C_α and from that in the triclinic crystal only 3.0825° for N_1−Pb−N_1. As has been noticed by Papageorgiou,[40] an obvious difference in the structure of PbPc exists between the monoclinic and triclinic forms: Strong intermolecular interactions are present and the PbPc molecules are more closely packed together in the former form, whereas weak intermolecular interactions and the molecules overlap only in the region of the benzene rings in the latter form. Our result in the structure of compound **1**, calculated in a vacuum system with only C_{4v} molecular symmetry restriction, can thus be reasonably considered as an intermediate between the monoclinic and triclinic crystals.

The main calculated structure parameters of PbPc(α-OC_5H_{11})$_4$ (**3**) together with the X-ray crystallography data are listed in Table 2, and their differences are compared in Figure 3. The biggest difference in bond length between the calculated and experimental data is only 0.0846 Å for C_2−C_3, and the smallest

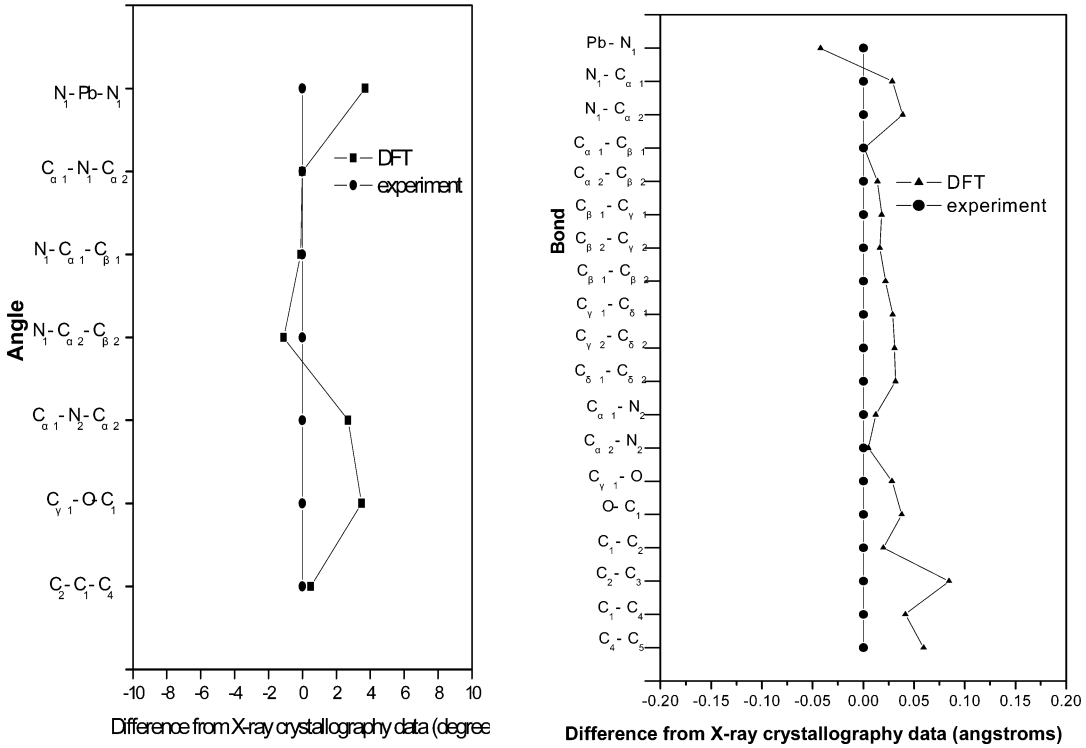

Figure 3. Comparison of main calculated bond lengths and bond angles with the X-ray crystallography data for $PbPc(\alpha\text{-}OC_5H_{11})_4$ (**3**).

one is 0.0009 Å for $C_{\alpha 1}-C_{\beta 1}$, indicating that the results obtained from the DFT method at the B3LYP basis set correspond very well with those of the experimental ones. It is worth mentioning that among the major computed 19 bond lengths, only the one of $Pb-N_1$ takes a smaller value compared with that obtained from the X-ray crystallography data, whereas the others are slightly larger than the experimental ones, suggesting that the difference found in this $Pb-N_1$ bond length does not result from the calculation method. In the single crystal, one molecule of **3** is surrounded by many other molecules including the molecules of the same compound and chloroform,[28] which inhibit the expansion of the phthalocyanine central cavity due to the interaction of this phthalocyanine ligand involved with other surrounding molecules. However, the simulated structural data are calculated for one molecule in gas phase without any other molecules surrounding it. During the optimization process the lead atom can sit atop of the ligand much deeper because of the free expansion of this phthalocyanine central cavity than in the crystal. As a result, the calculated $Pb-N_1$ bond length is slightly shortened in comparison with that in the crystal. The distance from the lead atom to the plane formed by four isoindole nitrogen atoms is 1.3101 Å according to the X-ray crystallography result, which is shortened to 1.1393 Å on the basis of our simulated result. As for the main bond angles shown in Table 2 and Figure 3b, the biggest difference between the simulated and experimental results comes from N_1-Pb-N_1 with a departure of 3.7° followed by $C_{\gamma 1}-O-C_1$ with 3.5°, whereas the smallest difference is from $C_{\alpha 1}-N_1-C_{\alpha 2}$ with a coincident equality. As was mentioned by many other investigators, the bond angle has a much larger error than the bond length does in the molecular simulation. This is also true in the present case as is clearly shown in Figure 3. Again, the good agreement in the structural data obtained by the DFT method with the experimental results for compound **3** indicates that our calculation method is reliable for simulating a large molecule with 121 atoms including the big lead atom.

The introduction of four ethyloxy and 3-pentyloxy groups at the α-positions of the phthalocyanine ligand for compounds **2** and **3**, respectively, induces significant changes in the structures compared with **1**. On the basis of our calculation results, compound **1** employs the C_{4v} molecular symmetry, with a C_4 axis going through the lead atom and the center of four isoindole nitrogen atoms, and with four symmetry planes including the C_4 axis. However, incorporation of four alkoxy groups at the nonperipheral positions of the phthalocyanine ring in **2** and **3** makes the four symmetry planes disappear and diminishes the molecular symmetry to C_4. Along with the lowering of the molecular symmetry from C_{4v} in **1** to C_4 in **2** and **3**, the intrinsic chiral property appears for the molecules of the latter two complexes. Four alkoxy groups at the nonperipheral positions of the phthalocyanine ligand also induce apparent torsion of the isoindole units in **2** and **3** due to the steric hindrance of ethyloxy or 3-pentyloxy groups. As shown in Figure 1, **1** and its analogues **2** and **3** have nonplanar "shuttle-cock" structures. The ethyl chains of the ethyloxy groups in **2** extending to the outside of isoindole unit planes, which form the feather part of the shuttle-cock, parallel with isoindole unit planes. In the molecule of **3**, the pentyl chains of the 3-pentylxoy groups are approximately perpendicular to the isoindole units. In the direction perpendicular to the C_4 axis and parallel to the isoindole units, tetra-substitution of alkoxy groups at the nonperipheral positions of the phthalocyanine ring also makes the isoindole units twist in **2** and **3**. As clearly displayed in Figure 1, for both complexes **2** and **3**, the bond lengths of the isoindole units on the side of the alkoxy group are apparently larger than those on the other side without a substituent. In **2**, the biggest difference in the bond length of the same isoindole unit between the bonds on the side with ethyloxy group and those on the other side without substituent amounts to 0.0179 Å for $C_\beta-C_\gamma$, whereas the smallest difference is only 0.0063 Å for $C_\gamma-C_\delta$. In **3**, they are 0.0149 Å for $C_\beta-C_\gamma$ and 0.0024 Å for $C_\alpha-C_\beta$, respectively. These results indicate that the twist of the isoindole units in both compounds is not large. Another

TABLE 3: Atomic Charges (in e) for PbPc (1), PbPc(α-OC_2H_5)$_4$ (2), and PbPc(α-OC_5H_{11})$_4$ (3) (Refer to Figure 1)

atom	Pb	N_1	$C_{\alpha1}$	$C_{\alpha2}$	$C_{\beta1}$	$C_{\beta2}$	$C_{\gamma1}$	$C_{\gamma2}$	$C_{\delta1}$	$C_{\delta2}$
1	1.42834	−0.75015	0.46793		−0.07300		−0.17976		−0.20461	
2	1.42393	−0.74818	0.47033	0.47127	−0.13701	−0.05954	0.36156	−0.19464	−0.23282	−0.19234
3	1.42423	−0.75086	0.46933	0.46366	−0.11502	−0.05461	0.36687	−0.20470	−0.28974	−0.18675

atom	N_2	$H_{\alpha2}$	$H_{\beta1}$	$H_{\beta2}$	O	C_1	C_2	C_3	C_4	C_5
1	−0.54286	0.23515	0.22226							
2	−0.56308	0.23335	0.23576	0.22418	−0.60138	−0.04018	−0.64679			
3	−0.53044	0.23605	0.21806	0.22001	−0.58576	0.15010	−0.42644	−0.63540	−0.41732	−0.63493

N_1: nitrogen atom joined to the central metal; N_2: nitrogen atom not joined to the central metal; α *β γ δ* mean carbon atoms in isoindole units beginning from N_1; H_α: hydrogen atom joined to C_γ; H_β: hydrogen atoms joined to C_δ; the subscript 1 on carbon atom refer to carbon atoms at the same side of oxygen atom, the subscript 2 on carbon atom refer to carbon atoms at the contrary side of oxygen atom, the same to hydrogen atoms; C_1: carbon atom in substituents joined to oxygen atom, C_2 and C_4 both joined to C_1 atom and C_2 C_3 at the same side of lead atom, C_4 and C_5 at the other side for *c* molecular. (see Figure 1).

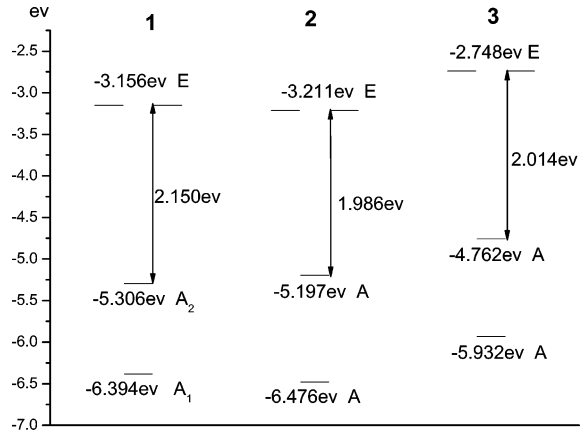

Figure 4. Orbital energies of the HOMO-1, HOMO, LUMO, and LUMO+1 orbitals of PbPc (**1**), PbPc(α-OC_2H_5)$_4$ (**2**), and PbPc(α-OC_5H_{11})$_4$ (**3**).

effect due to alkoxy substituents at four of the eight nonperipheral positions of phthalocyanine shown in the molecular structure is the difference in bond length between the two bonds connecting to the aza nitrogen atom. For instance in compound **2**, the $N_2-C_{\alpha1}$ bond length is about 0.0011 Å shorter than that of $N_2-C_{\alpha2}$. In **3**, these two bond lengths are equal by chance. It is worth noting again that these data are also in good correspondence with the experimental results, especially for compound **3**.[28]

As can be expected, the change in the structural data of isoindole units induced by introducing four alkoxy groups at the peripheral positions of phthalocyanine ligand in **2** and **3** naturally leads to the change in the structural data that are related with the central lead atom. As also listed in Figure 1, the average $Pb-N_1$ coordination bond lengths are 2.3343, 2.3366, and 2.3336 Å, respectively, for **1**, **2**, and **3** according to our calculation results, whereas the average N_1-Pb-N_1 angles in the three complexes amount to 76.1, 76.3, and 76.2°. These data suggest that no significant change is induced by the alkoxy groups at the nonperipheral positions of the phthalocyanine ligand due to the increased distance from the position that alkoxy substitution takes place. However, the distance of the lead away from the plane formed by the four isoindole nitrogen atoms changes obviously along with the substitution, which is 1.1448, 1.1364, and 1.1393 Å for **1**, **2**, and **3**, respectively.

Molecular Orbital Energies and Atomic Charges. Figure 4 shows the calculated energy levels of HOMO-1, HOMO, LUMO, and LUMO+1 orbitals of compounds **1**−**3**. The energy of HOMO decrease in the order of **1** < **2** < **3**. The LUMO and LUMO+1 orbitals are degenerate with the energy order of **2** < **1** < **3**. Therefore the HOMO−LUMO gap is the largest for **1**, 2.150 eV, and the smallest for **2**, 1.986 eV, with **3** intermediate between them, 2.014 eV. It is noteworthy that the values of HOMO−LUMO gap for these phthalocyaninato lead complexes are very important for getting information of their electronic absorptions, which reflect the energy necessary for the transition of an electron from the HOMO to the LUMO of corresponding compounds and therefore should correlate with the lowest energy optical transition in the electronic absorption spectrum of Pb(Pc′) [Pc′ = Pc, Pc(α-OC_2H_5)$_4$, Pc(α-OC_5H_{11})$_4$]. As detailed below, the diminished trend observed for the HOMO−LUMO gap value of phthalocyaninato lead complexes in the order from PbPc (**1**), Pb_2Pc(α-OC_5H_{11})$_4$ (**3**), and PbPc(α-OC_2H_5)$_4$ (**2**) is in good agreement with the red-shift of the Q absorption band of these compounds, where the Q-band position is determined at 625 for **1**, 673 for **3**, and 677 nm for **2** according to our calculation on the UV−vis spectra.

Table 3 lists the atomic charges (in e), calculated with NBO population method, of the skeleton atoms for **1**−**3**. The charge distributed to the lead atom for all three compounds is positive and has the coincident order with the distance of lead atom away from the plane formed by the four isoindole nitrogen atoms, **1** > **3** > **2**. It should be pointed out that although the lead sits closer to the phthalocyanine ring in compounds **2** and **3** than in **1**, which suggests the stronger metal−ligand reciprocity, the atomic charge for lead in **2** and **3** is still less positive than that in **1**. $C_\alpha1$ atoms have positive charge for the three complexes in the order of **2** > **3** > **1**. Comparison between the atomic charges for the $C_{\alpha1}$ and $C_{\alpha2}$ atoms, Table 3, reveals that introduction of alkoxy substituents makes $C_{\alpha1}$ have more positive charge for **2** and **3** than **1**. However, the $C_{\alpha2}$ atoms of **2** have more positive charge than **1** but those of **3** less positive charge than **1**. Except for the negative charge distributed to the $C_{\beta1}$ as well as the $C_{\beta2}$ atoms, the same trend on the atomic charge with that of $C_{\alpha1}$ atoms have been found for the $C_{\beta1}$ atoms for the three complexes, but the charge on $C_{\beta2}$ atoms for **2** and **3** are much less than that of $C_{\beta1}$, and even less than that of **1**, due to the alkoxy substitution to the $C_{\beta1}$ atoms. The $C_{\gamma2}$ atoms present negative charge, increasing in the order of **1** < **2** < **3**. In contrast, the $C_{\gamma1}$ atoms of **2** and **3** present positive charge due to the direct connection to the electronegative oxygen atoms. The negative charge of $C_{\delta1}$ atoms increases and that of $C_{\delta2}$ decreases from **1** to **3**. The expected trend according to that of Pb and C_α atomic charges for the negative charge of N_1 atoms was not found for these compounds. The negative charge of N_2 atoms shows the same trend with that of $C_{\alpha2}$ atoms in the order **2** > **1** > **3**. The oxygen atoms of **2** have more negative charge than **3**. For **2**, both the carbon atoms in the side ethyloxy substituents have negative charge. All of the carbon atoms, except the C_1 atoms directly connected to the oxygen atoms, in

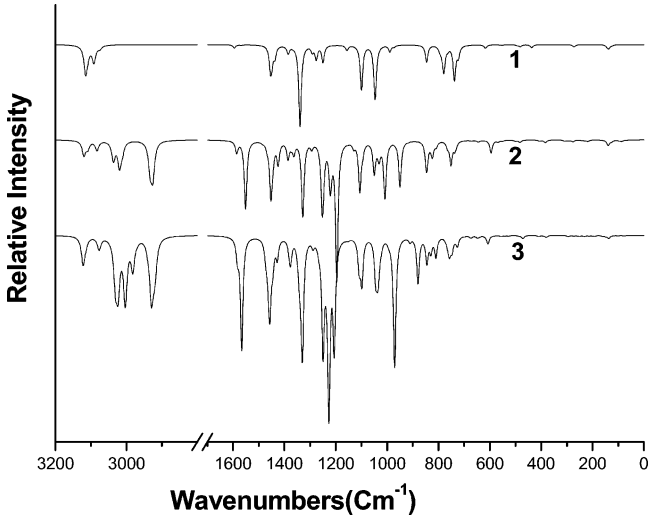

Figure 5. Simulated IR spectra of PbPc (**1**), PbPc(α-OC_2H_5)$_4$ (**2**), and PbPc(α-OC_5H_{11})$_4$ (**3**).

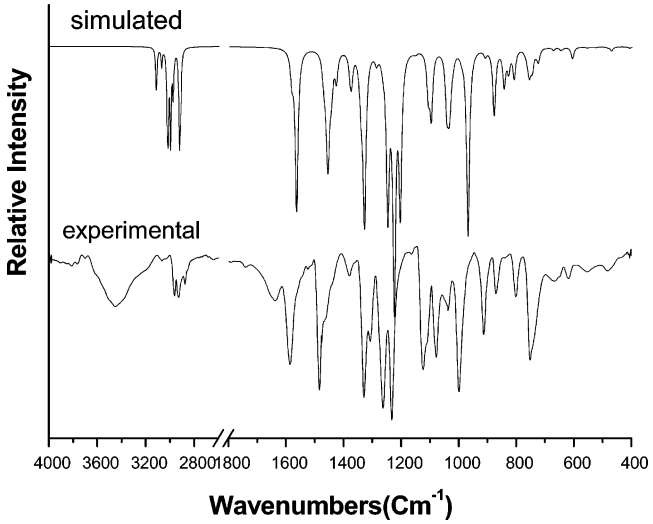

Figure 6. Comparison of the simulated and experimental IR spectra of PbPc(α-OC_5H_{11})$_4$ (**3**).

the 3-pentyloxy groups of **3** present negative charge. Another point worth to mention is that C_2 and C_3 atoms that are in the upside of isoindole plane show more negative charge compared with C_4 and C_5 atoms that are in the downside of the isoindole plane.

Infrared Spectra. The calculated infrared spectra of **1**−**3** are shown in Figure 5. The calculated data are scaled by the factor 0.9614[35] and dealt by fitting Lorentzian line shape. As shown in this figure, the number of vibrational modes increases along with the increase of alkoxy side chains from **1** to **2** and **3**. In comparison with the simulated spectrum of compound **1**, in the IR spectra of **2** and **3**, the most noticeable difference appears in the region of 2800−3200 cm^{-1}. Only two relatively weak peaks at 3092 and 3114 cm^{-1} are observed in the simulated spectrum of PbPc (**1**), which can be attributed to the benzene ring C−H stretching and swing with assistance of animated pictures produced based on the normal coordinates.[41] However, in addition to these vibrations, a couple of new peaks appear in this region, from 2926 to 3036 cm^{-1}, for compounds **2** and **3**, which are clearly due to the symmetrical and asymmetrical C−H stretching modes of the ethyloxy or 3-pentyloxy groups. The vibration peaks below 1700 cm^{-1} for these complexes are quite complicated and actually the mixture of many interrelated vibrational modes. The strongest peak for **2** locates at 1196 cm^{-1} due to the $C_{\gamma 1}$−O unsymmetrical stretching mixed with vibration of phthalocyanine skeleton, which blue-shifts to 1227 cm^{-1} for compound **3** due to the fact that the C_1 atoms of the side chains connected to the O atoms in **3** are tertiary carbons which experience a larger steric hindrance than the secondary carbons in **2**, and therefore, more inhibition occurs at the stretching vibration of C_1−O in **3** than in **2**. The fact that no peak near 1200 cm^{-1} is observed for **1** proves our identification that the strongest peak at 1196 and 1227 cm^{-1} in the IR spectra of **2** and **3**, respectively, is mainly due to the $C_{\gamma 1}$−O unsymmetrical stretching together with some contribution from the phthalocyanine skelecton vibration. For the unsubstituted analogue PbPc (**1**), the strongest peak appears at 1339 cm^{-1} contributed by benzene C−C stretching and C_α−N_2 stretching, which also exists in the spectra of **2** and **3** but takes a very slightly blue shift due to the alkoxoy substituents. It is noteworthy that the additional intense peak observed at 1551 and 1566 cm^{-1} for **2** and **3**, respectively, is also due to the vibrational modes associated with the oxygen atoms with the assistance of animated pictures produced based on the

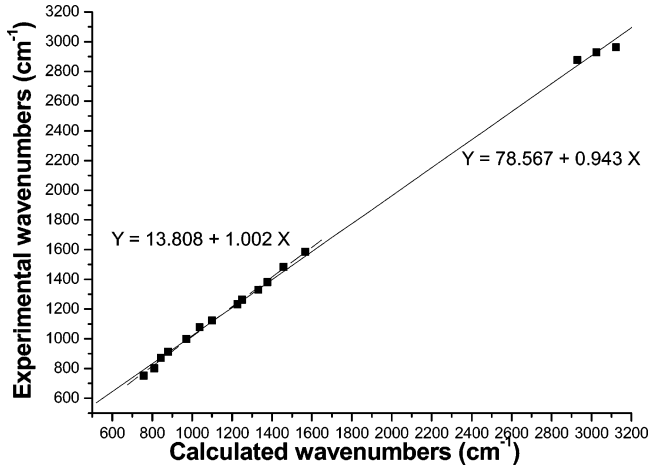

Figure 7. Consistency of the wavenumbers of the calculated and experimental IR spectra main peaks of PbPc(α-OC_5H_{11})$_4$ (**3**), short dash line indicates the consistency of peaks between 1800 and 400 cm^{-1}.

normal coordinates. It thus can be found that despite of the complexity in the IR vibrational spectra of substituted-phthalocyaninato lead complexes, most of the vibration modes can be identified and assigned by comparison with those of the unsubstituted analogue according to our calculation results.

To ensure the calculated results, the calculated and experimental IR spectra of compound **3** are compared in Figure 6. It can be seen from this figure that the IR spectrum of **3** obtained by calculation corresponds well with that recorded experimentally. Figure 7 gives the intuitional correspondence relationship of the calculated and experimental data by fitting them to a linear function. The slope of the line is 0.943 and the intercept only 78, showing good consistency between the calculated and experimental data. When the peaks in the far IR region over 2800 cm^{-1}, which are too separated from the other vibrations, are ignored, the slope of the line becomes 1.002 and the intercept 14, indicating further improved consistency. These results suggest that different scale factors for different vibration bands are needed in simulating the calculated IR spectrum. However, seeking scale factors for every wave band is such boring work that very few investigators have done it.[42,43] Usually, the scale factor found in the middle course was chosen as a general one used for simulation.[31,44,45]

Raman Spectra. The calculated Raman spectra of **1**−**3** are shown in Figure 8. Similar to the IR spectra, the calculated

TABLE 4: Calculated UV−Vis Spectra of PbPc (1), PbPc(α-OC_2H_5)$_4$ (2), and PbPc(α-OC_5H_{11})$_4$ (3)

1			2			3		
a	b	c	a	b	c	a	b	c
625 (0.62)	E	16.03%130A_1→136^{LUMO}E* 23.60%133A_1→136^{LUMO}E* 59.53%134$^{HOMO}A_2$→135^{LUMO}E*	677 (0.70)	E	12.21%172A→184^{LUMO}E* 15.43%181A→184^{LUMO} E* 55.62%182^{HOMO}A→183^{LUMO} E* 24.11%182^{HOMO}A→184^{LUMO} E*	673 (0.73) [751]^d	E	13.19%222A→232^{LUMO}E* 20.12%229A→232^{LUMO} E* 60.84%230^{HOMO}A→231^{LUMO} E*
472 (0.18)	E	16.85%130A_1→136^{LUMO}E* 63.16%133A_1→136^{LUMO} E* 12.45%134$^{HOMO}A_2$→135^{LUMO}E*	470 (0.18)	E	11.33%172A→183^{LUMO} E* 10.60%176A→184^{LUMO} E* 58.44%181A→183^{LUMO} E* 28.13%181A→184^{LUMO} E*	478 (0.24)	E	12.40%222A→232^{LUMO} E* 10.81%224A→231^{LUMO} E* 24.14%229A→231^{LUMO} E* 58.98%229A→232^{LUMO} E*
			442 (0.22)	E	11.30%177B→183^{LUMO} E* 65.44%180B→183^{LUMO} E* 15.93%180B→184^{LUMO} E*	442 (0.21) [432]^d	E	29.94%225B→231^{LUMO} E* 21.29%225B→232^{LUMO} E* 44.22%228B→231^{LUMO} E* 37.74%228B→232^{LUMO} E*
352 (1.29)	E	10.27%121A_2→136^{LUMO} E* 10.27%125B_1→136^{LUMO} E* 63.03%130A_1→135^{LUMO} E*	371 (0.35)	E	34.55%172A→183^{LUMO} E* 25.46%176A→183^{LUMO} E* 52.52%176A→184^{LUMO} E*	365 (0.30)	E	32.28%222A→232^{LUMO} E* 16.06%223B→231^{LUMO} E* 13.27%223B→232^{LUMO} E* 57.12%224A→231^{LUMO} E*
316 (0.36)	E	17.58%122A_1→135^{LUMO} E* 65.25%134$^{HOMO}A_2$→139E*	345 (0.97)	E	10.07%169A→183^{LUMO} E* 14.37%172A→183^{LUMO} E* 53.12%172A→184^{LUMO} E* 29.84%176A→183^{LUMO} E*	338 (1.13) [333]^d	E	55.28%222A→232^{LUMO} E* 28.93%224A→231^{LUMO} E*

[a] Wavelength(nm) and corresponding oscillator strength (in parentheses). [b] Symmetry of the excited states. [c] The nature of electronic transitions, the percents are contributions of each transition, the numbers before the orbital are numbers of the corresponding orbital, * means the orbital is antibonding orbital. [d] Experimental data taken from ref 28.

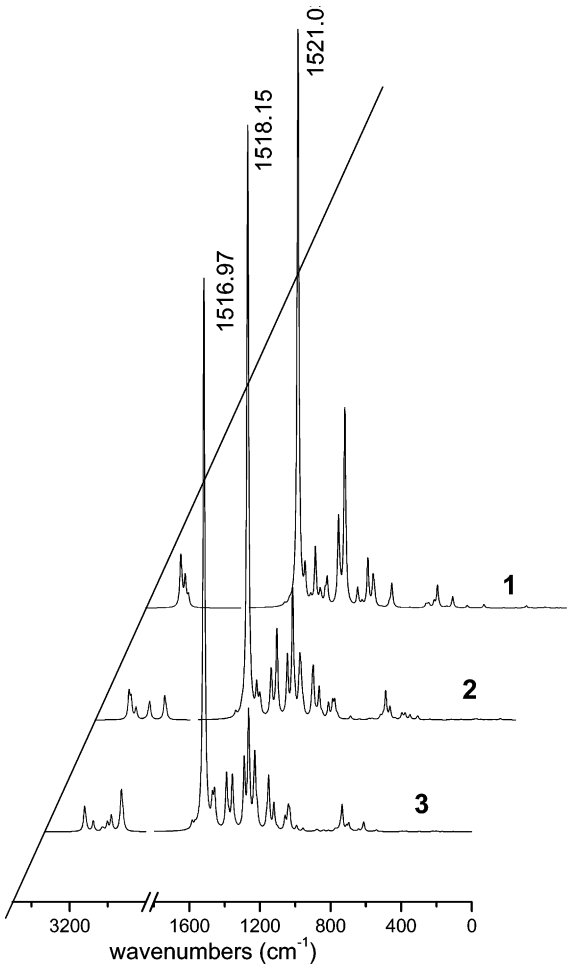

Figure 8. Simulated Raman spectra of PbPc (**1**), PbPc(α-OC_2H_5)$_4$ (**2**), and PbPc(α-OC_5H_{11})$_4$ (**3**).

Raman data are scaled also by the factor of 0.9614 and dealt by fitting Lorentzian line shape. The strongest peaks of the three complexes are C−N_1−C symmetry in plane bending and C−N_2 asymmetry stretching mixed with C−C and C−N_1 stretching, appearing at 1521, 1518, and 1517 cm^{-1}, which contains no contribution from the alkoxy substituent vibrations in **2** and **3**.

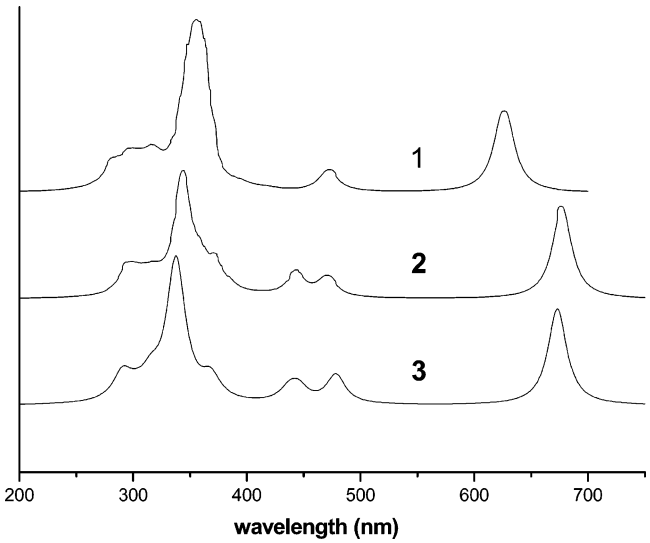

Figure 9. Simulated UV−vis spectra of PbPc (**1**), PbPc(α-OC_2H_5)$_4$ (**2**), and PbPc(α-OC_5H_{11})$_4$ (**3**).

With assistance of animated pictures produced based on the normal coordinates, other Raman peaks can also be easily assigned. Like in the IR spectra, there are more peaks in the Raman spectra of **2** and **3** than in **1** due to the diminished molecular symmetry. As also expected, along with the increased atomic number from **1** to **2** to **3**, the number of Raman vibration peaks increases in the same order.

UV−Vis Spectra. Figure 9 shows the simulated electronic absorption spectra of the three phthalocyaninato lead complexes (**1**−**3**), and Table 4 organizes the main peaks, their corresponding oscillator strength and symmetries, and the nature of electronic transitions. The results obtained by TDDFT calculations, Table 4, show that the Q-band of these three complexes, **1**−**3**, is mainly due to the electronic transition from HOMO to LUMO. Therefore, just in line with the molecular orbital energy calculation result described above, the Q-band of **1** appears at the higher energy side than that of **2** and **3** due to the larger energy gap of this compound, whereas the Q-band of the latter two complexes locates almost at the same position because of their close orbital energy gap. As can be seen, the Soret

absorption at ca. 350 nm for **1** is more intense than that for **2** and **3** due to the larger oscillator strength according to the calculation. One absorption appears at 472 nm for the unsubstituted phthalocyaninato lead compound **1** due to the electron transition from HOMO-1 to LUMO according to the calculation, which however was not observed in the electronic absorption spectrum of PbPc (**1**). However, for the substituted phthalocyaninato lead analogues **2** and **3**, another peak is also observed at 442 nm in addition to the one at 470 and 478 nm, respectively. It is worth mentioning that the absorption band at 442 nm, which is common for alkoxy-substituted phthalocyaninato compounds, can be attributed to the n-π^* transition.

According to the experimental result,[28] there appear three main absorption bands at 333, 432, and 751 nm in the UV−vis spectra of **3**. The calculated absorption band at 338 nm for **3** is corresponding to the observed Soret absorption at 333 nm. Corresponding to the observed peak at 432 nm, there are two absorption bands at 442 and 478 nm according to our calculation. The former absorption at 442 nm is attributed to the n-π^* transition due to 3-pentyloxy groups and the latter one is absent in the experimental UV−vis spectrum, in line with the result obtained for the unsubstituted PbPc (**1**). It is noteworthy that the calculated Q-band for **3** appears at 673 nm, which is a bit of farther from the observed Q-band at 751 nm.

Conclusion

An accurate description of the molecular structures, molecular orbital energy gaps, atomic charges, IR and Raman spectra, and UV−vis spectra of phthalocyaninato lead complexes has been provided by DFT and TDDFT calculations. The calculated results are in good agreement with the experimental data, indicating that the method and basis set selected are feasible for calculating such a large molecule as phthalocyaninato lead complexes involving 121 atoms.

Acknowledgment. Financial support from the Natural Science Foundation of China (Grant No. 20325105, 20431010), National Ministry of Science and Technology of China (Grant No. 2001CB6105), and Ministry of Education of China, Shandong University for J. Jiang is gratefully acknowledged. We also are grateful to the Shandong Province High Performance Computing Centre for a grant of computer time.

Supporting Information Available: All the calculated geometry structures, atomic numbers, structure figures of calculated HOMO and LUMO molecular orbitals of of **1**−**3**, and UV−vis spectra of PbPc (**1**) calculated in different methods. This material is available free of charge via the Internet at http://pubs.acs.org.

References and Notes

(1) Mckeown, N. B. *Phthalocyanine Materials: Synthesis, Structure and Function*; Cambridge University Press: Cambridge, England, 1998.
(2) Lever, A. B. P.; Leznoff, C. C. *Phthalocyanine: Properties and Applications*; VCH: New York, 1989−1996; Vols. 1−4.
(3) Kadish, K. M.; Smith, K. M.; Guilard, R. *The Porphyrin Handbook*; Academic Press: San Diego, CA, 2000−2003; Vols. 1−20.
(4) Gregory, P. *High-Technology Applications of Organic Colorants*; Plenum Press: New York, 1991.
(5) Gregory, P. *J. Porphyrins Phthalocyanines* **2000**, *4*, 432.
(6) Ao, R.; Kilmmert, L.; Haarer, D. *Adv. Mater.* **1995**, *7*, 495.
(7) Birkett, D. *Chem. Ind.* **2000**, 178.
(8) Moser, F. H.; Thomas, A. L. *The Phthalocyanines; Vols. 1 and 2, Manufacture and Applications*; CRC Press: Boca Raton, FL, 1983.
(9) Wöhrle, D.; Meissner, D. *Adv. Mater.* **1991**, *3*, 129.
(10) Eichhorn, H. *J. Porphyrins Phthalocyanines.* **2000**, *4*, 88.
(11) Wright, J. D. *Prog. Surf. Sci.* **1989**, *31*, 1.
(12) Snow, A. W.; Barger, W. R. *In Phthalocyanines: Properties and Applications*; Leznoff, C. C., Lever, A. B. P., Eds.; VCH: New York, 1989; pp 341−392.
(13) Nalwa, H. S.; Shirk, J. S. *In Phthalocyanines: Properties and Applications*; Leznoff, C. C., Lever, A. B. P., Eds.; VCH: New York, 1996; pp 79−182.
(14) Shirk, J. S.; Pong, R. G. S.; Flom, S. R.; Heckmann, H.; Hanack, M. *J. Phys. Chem.* **2000**, *104*, 1438.
(15) de la Torre, G.; Vázquez, P.; AgullóPez, F.; Torres, T. *J. Mater. Chem.* **1998**, *8*, 1671.
(16) LukCentyanets, E. A. *J. Porphyrins Phthalocyanines.* **1999**, *3*, 424.
(17) H. Hasrar, H.; van Lier, J. E. *Chem. Rev.* **1999**, *99*, 2379.
(18) Cosomelli, B.; Roncuccin, G.; Dei, D.; Fantetti, L.; Ferroin, F.; Ricci, M.; Spinelli, D. *Tetrahedron* **2003**, *59*, 10025.
(19) Beltrán, H. I.; Esquive, R.; Sosa-Sánchez, A.; Sosa-Sánchez, J. L.; Höpfl, H.; Barba, V.; Farfan, N.; Garcia, M. G.; Olivares-Xometl, O.; Zamudio-Rivera, L. S. *Inorg. Chem.* **2004**, *43*, 3555.
(20) Bian, Y.; Wang, R.; Jiang, J.; Lee, C.-H.; Wang, J.; Ng, D. K. P. *Chem. Commun.* **2003**, 1194.
(21) Bian, Y.; Wang, R.; Wang, D.; Zhu, P.; Li, R.; Dou, J.; Liu, W.; Choi, C.-F.; Chan, H.-S.; Ma., C.; Ng, D. K. P.; Jiang, J. *Helv. Chim. Acta*, **2004**, *87*, 2581.
(22) Bian, Y.; Li, L.; Wang, D.; Choi, C.-F.; Cheng, D. F. F.; Zhu, P.; Li, R.; Dou, J.; Wang, R.; Pan, N.; Ma, C.; Ng, D. K. P.; Kobayashi, N.; Jiang, *Eur. J. Inorg. Chem.*, in press.
(23) Ukei, K. *Acta Crystallogr.* **1973**, *B29*, 2290.
(24) Ukei, K. *J. Phys. Soc. Jpn.* **1976**, *40*, 140.
(25) Iyechika, Y.; Yakushi, K.; Ikemoto, I.; Kuroda, H. *Acta Crystallogr.* **1982**, *B38*, 766.
(26) Przyborowski, F.; Hamann, C. *Cryst. Res. Technol.* **1982**, *17*, 1041.
(27) Bluhm, T. L.; Wagner, H. J.; Loutfy. R. O. *J. Mater. Sci. Lett.* **1983**, *2*, 85.
(28) Bian, Y.; Li, L.; Dou, J.; Cheng, D. Y. Y.; Li, R.; Ma, C.; Ng, D. K. P.; Jiang, J. *Inorg. Chem.* **2004**, *43*, 7539−7544.
(29) Burnham, P. M.; Cook, M. J.; Gerrard, L. A.; Heeney, M. J.; Hughes, D. L. *Chem. Commun.* **2003**, 2064.
(30) Ding, H. M.; Wang, S. Y.; Xi, S. Q. *J. Mol. Struct.*, **1999**, *475*, 175−180.
(31) Gong, X.; Xiao, H.; Tian, H. *J. Mol. Struct. (THEOCHEM)* **2002**, *593*, 93−100.
(32) Liao, M.; Kar, T.; Gorun, S. M.; Scheiner, S. *Inorg. Chem.* **2004**, *43*, 7151−7161
(33) Day, P. N.; Wang, Z. Q.; Pachter, R. *J. Mol. Struct. (THEOCHEM)* **1998**, *455*, 33−50.
(34) Peng, C.; Ayala, P. Y.; Schlegel, H. B.; Frisch, M. J. *J. Comput. Chem.* **1996**, *17*, 49.
(35) NIST Computational Chemistry Comparison and Benchmark Database, NIST Standard Reference Database Number 101 Release 10, May 2004, Editor: Russell D. Johnson, III. http://srdata.nist.gov/cccbdb.
(36) Frisch, M. J.; Trucks, G. W.; Schlegel, H. B.; Scuseria, G. E.; Robb, M. A.; Cheeseman, J. R.; Montgomery, Jr., J. A.; Vreven, T.; Kudin, K. N.; Burant, J. C.; Millam, J. M.; Iyengar, S. S.; Tomasi, J.; Barone, V.; Mennucci, B.; Cossi, M.; Scalmani, G.; Rega, N.; Petersson, G. A.; Nakatsuji, H.; Hada, M.; Ehara, M.; Toyota, K.; Fukuda, R.; Hasegawa, J.; Ishida, M.; Nakajima, T.; Honda, Y.; Kitao, O.; Nakai, H.; Klene, M.; Li, X.; Knox, J. E.; Hratchian, H. P.; Cross, J. B.; Bakken, V.; Adamo, C.; Jaramillo, J.; Gomperts, R.; Stratmann, R. E.; Yazyev, O.; Austin, A. J.; Cammi, R.; Pomelli, C.; Ochterski, J. W.; Ayala, P. Y.; Morokuma, K.; Voth, G. A.; Salvador, P.; Dannenberg, J. J.; Zakrzewski, V. G.; Dapprich, S.; Daniels, A. D.; Strain, M. C.; Farkas, O.; Malick, D. K.; Rabuck, A. D.; Raghavachari, K.; Foresman, J. B.; Ortiz, J. V.; Cui, Q.; Baboul, A. G.; Clifford, S.; Cioslowski, J.; Stefanov, B. B.; Liu, G.; Liashenko, A.; Piskorz, P.; Komaromi, I.; Martin, R. L.; Fox, D. J.; Keith, T.; Al-Laham, M. A.; Peng, C. Y.; Nanayakkara, A.; Challacombe, M.; Gill, P. M. W.; Johnson, B.; Chen, W.; Wong, M. W.; Gonzalez, C.; Pople, J. A. *Gaussian 03*, revision B.05; Gaussian, Inc.: Wallingford, CT, 2004.
(37) Sakata, M.; Sumimoto, M.; Gushima, M.; Fujimoto, H.; Matsuzaki, S. *Solid State Commun.* **2002**, *121*, 363−366.
(38) Ukei, K. *Acta Crystallogr., Sect. B: Struct. Crystallogr. Cryst. Chem.* **1973**, *B29*, 2290.
(39) Iyechika, K.; Yakushi, Y.; Ikemoto, I.; Kuroda, H. *Acta Crystallogr., Sect. B: Struct. Crystallogr. Cryst. Chem.* **1982**, *B38*, 766.
(40) Papageorgiou, N.; Ferro, Y.; Salomon, E.; Allouche, A.; Layet, J. M. *Phys. Rev. B*, **2003**, *68*, 235105.
(41) Zhang, X.; Zhang, Y.; Jiang, J. *Spectrochim. Acta Part A* **2004**, *60*, 2195−2200.
(42) Rauhut, G.; Pulay, P. *J. Phys. Chem.* **1995**, *99*, 3093.
(43) Kovacs, A.; Izvekov, V.; Keresztury, G.; Pongor, G. *Chem. Phys.* **1998**, *238*, 231−243.
(44) Gong, X.; Xiao, H.; Tian, H. Int. *J. Quantum Chem.* **2002**, *86*, 531−540.
(45) Thomas, S. R., III; Pawel, M. K.; Christine, A. P.; Ranjit, K.; Marek, Z. Z.; Thomas, G. S. *J. Phys. Chem. B* **2000**, *104*, 5020−5034.